A New Approach to Multicarrier Pulse Design for Doubly-Dispersive Channels

Phil Schniter*†
Dept. of Electrical Engineering, The Ohio State University, Columbus, OH.

Abstract

For doubly-dispersive channels, we propose a pulse-shaped multicarrier modulation scheme designed to yield an inter-symbol/inter-carrier interference (ISI/ICI) profile facilitating high-performance/low-complexity equalization. Specifically, sampled transmitter/receiver pulses are jointly optimized to maximize a particular signal to interference-plus-noise ratio. Two low-complexity iterative equalization algorithms are proposed which leverage the resulting ISI/ICI structure, one based on soft feedback and the other on hard feedback. Simulations indicate that the soft feedback algorithm achieves estimation performance close to the matched filter bound in most scenarios. Post-cursor ISI cancellation is also considered, and found to be appropriate when the delay spread is large.

1 Introduction

In non-trivial time- and frequency-selective environments, single carrier modulation requires long and quickly-adapting equalizers for inter-symbol interference (ISI) mitigation, leading to complicated/expensive receivers. Multi-carrier modulation (MCM) has thus emerged as an attractive alternative.

Orthogonal frequency-division multiplexing (OFDM) [1] is probably the most well-known MCM technique. Leveraging FFTs at the transmitter and receiver, its complexity is the lowest among spectrally-efficient MCM techniques. While the use of a cyclic prefix (CP) gives OFDM robustness to *time*-dispersive fading (at the expense of reduced spectral efficiency), CP-OFDM is often considered non-robust to *frequency*-dispersive fading, since this fading induces inter-carrier interference (ICI) in CP-OFDM (see, e.g., [2, 3] and references therein). This notion should be considered more carefully, however: while ICI mandates a more complex receiver, it also introduces beneficial Doppler-diversity [3–5]. In fact, it has been shown that, with appropriate ICI shaping, it is possible to leverage a large proportion of this diversity using a computationally efficient equalization scheme—one that requires only $\mathcal{O}(N)$ operations beyond the traditional CP-OFDM receiver [6, 7]. In other words, the benefits of ICI may outweigh the costs.

Various MCM techniques have been proposed over the years, some with the explicit goal of suppressing ISI/ICI in the presence of doubly-selective channels. In this latter class we find pulse-shaped FDM[1] (PS-FDM) [8–11] and OQAM-OFDM (see [12] and references therein).

*2015 Neil Avenue, Columbus, OH 43210. E-mail: schniter@ee.eng.ohio-state.edu
†This work supported by NSF CAREER grant 237037.
[1]We write "FDM" rather than "OFDM" because some pulse designs prevent orthogonality.

In PS-FDM, OFDM's traditionally rectangular pulse is replaced with a smoother pulse that has better time/frequency localization. PS-FDM is attractive in that it's implementation complexity is only marginally greater than that of CP-OFDM but has the disadvantage that its ISI/ICI suppression comes at the cost of reduced spectral efficiency [12]. OQAM-OFDM uses a clever application of offset-QAM which allows smoothly overlapping OQAM-OFDM symbols. The result is ISI/ICI suppression without any reduction in spectral efficiency. The implementation complexity of OQAM-OFDM can be substantially greater than that of CP-OFDM, however, because it requires filterbanks in addition to FFTs. In fact, OQAM-OFDM's complexity has been found to increase in proportion to its ISI/ICI suppression capabilities [12]. Finally, it is important to remember that, while PS-FDM and OQAM-OFDM are able to suppress ISI/ICI in doubly-selective environments, they are not able to eliminate it completely.

Motivated by [6,7], we propose a PS-FDM system whose pulse-shapes are designed to generate *controlled* ISI/ICI. The target ISI/ICI profile will be chosen to facilitate high-performance low-complexity equalization. In other words, we propose MCM design for ISI/ICI *shaping* rather than ISI/ICI suppression. In this work, PS-FDM is chosen in place of OQAM-OFDM for reasons of simplicity. A similar design based on OQAM-OFDM would be interesting, but is outside the scope of this paper.

We now mention three related works. Matheus and Kammeyer [10] also proposed a PS-FDM scheme in which ISI/ICI was tolerated and then mitigated using Viterbi detection. They did not design for a particular target ISI/ICI pattern, though, and simply assumed continuous Gaussian pulse shapes. Kozek and Molisch [11] designed continuous pulses matched to the statistics of a WSSUS Rayleigh-fading channel, though their aim was to suppress ISI/ICI completely rather than shape it. Sun [13] proposed CP-OFDM without a guard interval (i.e., rectangular pulses) and one-tap decision-feedback equalization (DFE) at the receiver to mitigate ISI/ICI. Our work differs from these in that we design discrete-time transmitter/receiver pulse sequences that are *jointly-SINR-optimal*, leveraging WSSUS doubly-selective channel statistics and measuring SINR relative to a carefully-chosen target ISI/ICI pattern. For equalization, we build on the iterative algorithms of [6, 7], which have been shown to exhibit performance near the matched-filter bound but with significantly less complexity than Viterbi detection.

Notation: We use $(\cdot)^t$ to denote transpose, $(\cdot)^*$ conjugate, and $(\cdot)^H$ conjugate transpose. $\mathcal{C}(\boldsymbol{b})$ denotes the circulant matrix with first column $\boldsymbol{b}$, $\mathcal{D}(\boldsymbol{b})$ the diagonal matrix created from vector $\boldsymbol{b}$, and $\boldsymbol{I}$ the identity matrix. We use $[\boldsymbol{B}]_{m,n}$ to denote the element in the m^{th} row and n^{th} column of $\boldsymbol{B}$, where row/column indices begin with zero. $\|\cdot\|_F$ denotes the Frobenius norm, and $\odot$ element-wise multiplication. Expectation is denoted by $\mathrm{E}\{\cdot\}$ and covariance by $\mathrm{Cov}\{\boldsymbol{b},\boldsymbol{c}\} := \mathrm{E}\{\boldsymbol{b}\boldsymbol{c}^H\} - \mathrm{E}\{\boldsymbol{b}\}\,\mathrm{E}\{\boldsymbol{c}^H\}$. Finally, $\delta(\cdot)$ denotes the Kronecker delta, and $\mathbb{Z}$ the set of integers.

2 System Model

At each index $i \in \mathbb{Z}$, a set of N coded QAM symbols $\{s_k^{(i)}\}$ is collected to form a multicarrier symbol $\boldsymbol{s}^{(i)} = [s_0^{(i)}, \ldots, s_{N-1}^{(i)}]^t$. These symbols are used to modulate pulsed carriers as follows:

$$t_n \;=\; \sum_{i=-\infty}^{\infty} a_{n-iN_s} \frac{1}{\sqrt{N}} \sum_{k=0}^{N-1} s_k^{(i)} e^{j\frac{2\pi}{N}(n-iN_s-N_o)k} \tag{1}$$

In (1), $\{a_n\}$ is the transmit pulse sequence, N_s is the multicarrier symbol interval, and $N_o \in \{0, \ldots, N-1\}$ delays the carrier origin relative to the pulse origin. The multipath channel is described by its time-variant discrete impulse response $h_{\mathsf{tl}}(n,l)$, defined as the time-n response

to an impulse applied at time $n-l$. We assume a causal impulse response of length of N_h. The signal observed by the receiver is then

$$r_n \;=\; \nu_n + \sum_{l=0}^{N_h-1} h_{\mathsf{tl}}(n,l)\,t_{n-l} \tag{2}$$

where ν_n denotes samples of additive white circular Gaussian noise (AWGN) with variance σ^2. Defining $r_n^{(i)} := r_{iN_s+n}$, $\nu_n^{(i)} := \nu_{iN_s+n}$, and $h_{\mathsf{tl}}^{(i)}(n,l) := h_{\mathsf{tl}}(iN_s+n,l)$, it can be shown that

$$r_n^{(i)} \;=\; \nu_n^{(i)} + \sum_{l=0}^{N_h-1} h_{\mathsf{tl}}^{(i)}(n,l) \sum_{\ell=-\infty}^{\infty} a_{\ell N_s+n-l} \frac{1}{\sqrt{N}} \sum_{k=0}^{N-1} s_k^{(i-\ell)} e^{j\frac{2\pi}{N}(n-l+\ell N_s-N_o)k} \tag{3}$$

To estimate the multicarrier symbol $\boldsymbol{s}^{(i)}$, the receiver employs the pulse $\{b_n\}$ as follows:

$$x_d^{(i)} \;=\; \frac{1}{\sqrt{N}} \sum_n r_n^{(i)} b_n e^{-j\frac{2\pi}{N}d(n-N_o)} \tag{4}$$

Here again N_o delays the carrier origin relative to the pulse origin. Note that this system reduces to CP-OFDM with $N_o = N_s - N$, $\{a_n\}_{n=0}^{N_s-1} = 1$, and $\{b_n\}_{n=N_o}^{N_s-1} = 1$ (else $a_n = b_n = 0$). Note also that $N_g := N_s - N$ is analogous to CP-OFDM guard interval.

Plugging (3) into (4), we find

$$x_d^{(i)} \;=\; w_d^{(i)} + \sum_{\ell} \sum_{k=0}^{N-1} \breve{h}_{\mathsf{df}}^{(i,\ell)}(d-k,k)\, s_k^{(i-\ell)} \tag{5}$$

where

$$w_d^{(i)} \;:=\; \frac{1}{\sqrt{N}} \sum_n b_n \nu_n^{(i)} e^{-j\frac{2\pi}{N}d(n-N_o)} \tag{6}$$

$$\breve{h}_{\mathsf{df}}^{(i,\ell)}(d,k) \;:=\; \frac{1}{N} \sum_n \sum_{l=0}^{N_h-1} h_{\mathsf{tl}}^{(i)}(n,l) b_n a_{\ell N_s+n-l}\, e^{-j\frac{2\pi}{N}d(n-N_o)} e^{-j\frac{2\pi}{N}k(l-\ell N_s)} \tag{7}$$

Equation (5) indicates that $\breve{h}_{\mathsf{df}}^{(i,\ell)}(d,k)$ can be interpreted as the response, at time i and subcarrier $k+d$, to a frequency-domain impulse applied at time $i-\ell$ and subcarrier k.

In practice we implement finite-duration causal pulses $\{a_n\}$ and $\{b_n\}$ of length N_a and N_b, respectively, implying that only a finite number of terms in the set $\{\breve{h}_{\mathsf{df}}^{(i,\ell)}(d,k), \ell \in \mathbb{Z}\}$ will be non-zero. Specifically, (7) implies that non-zero terms result from indices ℓ which satisfy $0 \le \ell N_s + n - l \le N_a - 1$ for some $n \in \{0,\ldots,N_b-1\}$ and some $l \in \{0,\ldots,N_h-1\}$. It is straightforward to show that $\breve{h}_{\mathsf{df}}^{(i,\ell)}(d,k)$ is non-zero for $\ell \in \{-L_{\mathsf{pre}},\ldots,L_{\mathsf{pst}}\}$ where $L_{\mathsf{pre}} = \lfloor \frac{N_b-1}{N_s} \rfloor$ and $L_{\mathsf{pst}} = \lfloor \frac{N_a+N_h-2}{N_s} \rfloor$.

With the definitions $\boldsymbol{x}^{(i)} := [x_0^{(i)},\ldots,x_{N-1}^{(i)}]^t$, $\boldsymbol{w}^{(i)} := [w_0^{(i)},\ldots,w_{N-1}^{(i)}]^t$, and $[\breve{\mathcal{H}}^{(i,\ell)}]_{d,k} := \breve{h}_{\mathsf{df}}^{(i,\ell)}(d-k,k)$, (5) implies the linear time-varying (LTV) multiple-input multiple-output (MIMO) system

$$\boldsymbol{x}^{(i)} \;=\; \boldsymbol{w}^{(i)} + \sum_{\ell=-L_{\mathsf{pre}}}^{L_{\mathsf{pst}}} \breve{\mathcal{H}}^{(i,\ell)} \boldsymbol{s}^{(i-\ell)}. \tag{8}$$

In the sequel we assume wide-sense stationary uncorrelated scattering (WSSUS) [14] so that $\mathrm{E}\{h_{\mathsf{tl}}(n,l)h_{\mathsf{tl}}^*(n-q,l-m)\} = r_{\mathsf{t}}(q)\sigma_l^2\delta(m)$. Here, $r_{\mathsf{t}}(q)$ denotes the normalized autocorrelation (i.e., $r_{\mathsf{t}}(0)=1$) and σ_l^2 the variance of the l^{th} lag.

3 Pulse and Window Design

The choice of $\{a_n\}$ and $\{b_n\}$ affect the ISI/ICI patterns of the MIMO system (8). For example, it is well known that the CP-OFDM choices yield an system for which ISI and ICI vanish *if* the channel is LTI with delay spread $N_h \leq N_s - N + 1$. The absence of ISI/ICI greatly simplifies equalization; this is the classical motivation for CP-OFDM and, more generally, orthogonal MCM. When the channel is LTV or it is impractical to enforce $N_h \leq N_s - N + 1$, however, no choice of $\{a_n\}$ and $\{b_n\}$ is capable of completely suppressing both ISI and ICI. Our strategy is to choose $\{a_n\}$ and $\{b_n\}$ which impart a particular structure on the effective channel response $\breve{\mathcal{H}}^{(i,\ell)}$. The ideal target ICI/ISI pattern should allow high-performance/low-complexity equalization while being (nearly) attainable for some choice of $\{a_n\}$ and $\{b_n\}$.

3.1 ISI-Free Pulse Design

In this section, we focus on an ICI/ISI target that has a "cursor" coefficient $\breve{\mathcal{H}}^{(i,0)}$ with the banded structure illustrated in Fig. 1 and ISI coefficients $\{\breve{\mathcal{H}}^{(i,\ell)}\}_{\ell\neq 0}$ which equal zero. This choice is motivated by the lowpass nature of typical Doppler spectra (see [7]) and assumes that ISI can be effectively suppressed. With very long delay spread, it may be more appropriate to design pulses which allow post-cursor ISI and apply block decision feedback equalization; this is discussed in Sec. 3.2.

We design pulses according to the $\mathrm{SINR}(\boldsymbol{x}^{(i)}) := \mathcal{E}_{\mathsf{s}}/\mathcal{E}_{\mathsf{ni}}$ criterion, where signal energy $\mathcal{E}_{\mathsf{s}}$ and noise-plus-interference energy $\mathcal{E}_{\mathsf{ni}}$ are defined relative to the target. If we define $\mathcal{E}_{\mathsf{s},d}$ to be the energy contributed by $s_d^{(i)}$ to $x_d^{(i)}$, and if we define $\mathcal{E}_{\mathsf{ni},d}$ to be the energy contributed to $x_d^{(i)}$ by additive noise $w_d^{(i)}$, non-cursor symbols $\{s_d^{(j)}\}_{j\neq i}$, and non-neighboring co-cursor symbols $\{s_k^{(i)}\}_{k=0}^{d-D-1} \cup \{s_k^{(i)}\}_{k=d+D+1}^{N-1}$, then $\mathcal{E}_{\mathsf{s}} = \sum_d \mathcal{E}_{\mathsf{s},d}$ and $\mathcal{E}_{\mathsf{ni}} = \sum_d \mathcal{E}_{\mathsf{ni},d}$. Note that the energy contributed to $x_d^{(i)}$ by neighboring co-cursor symbols $\{s_k^{(i)}\}_{k=d-D}^{d-1} \cup \{s_k^{(i)}\}_{k=d+1}^{d+D}$ is considered neither signal nor interference, but rather a "don't care" quantity. In choosing $\boldsymbol{a} := [a_0, \ldots, a_{N_a-1}]^t$, we impose the average transmitted power constraint $\|\boldsymbol{a}\|^2 = N_s$, consistent with CP-OFDM.

From (5) and the description above, we have

$$\mathcal{E}_{\mathsf{s}} \;=\; \sum_{d=0}^{N-1} \mathcal{E}_{\mathsf{s},d} \;:=\; \sum_{d=0}^{N-1} \mathrm{E}\left\{ \left| \breve{h}_{\mathsf{df}}^{(i,0)}(0,d)\, s_d^{(i)} \right|^2 \right\} \;=\; \sum_{d=0}^{N-1} \mathrm{E}\left\{ \left| \breve{h}_{\mathsf{df}}^{(i,0)}(0,d) \right|^2 \right\}. \tag{9}$$

From (7) and our WSSUS assumption it can be shown that

$$\mathrm{E}\{|\breve{h}_{\mathsf{df}}^{(i,\ell)}(d,k)|^2\} \;=\; \frac{1}{N^2} \sum_{n,m=0}^{N_b-1} r_{\mathsf{t}}(n-m) b_n b_m^* e^{-j\frac{2\pi}{N}d(n-m)} \sum_{l=0}^{N_h-1} \sigma_l^2 a_{\ell N_s+n-l} a_{\ell N_s+m-l}^*, \tag{10}$$

implying that

$$\mathcal{E}_{\mathsf{s}} \;=\; \frac{1}{N} \sum_{n=0}^{N_b-1} \sum_{m=0}^{N_b-1} b_n b_m^* r_{\mathsf{t}}(n-m) \sum_{l=0}^{N_h-1} \sigma_l^2 a_{n-l} a_{m-l}^*. \tag{11}$$

Equation (11) can be put in the quadratic forms (12) and (13),

$$\mathcal{E}_{\mathsf{s}} \;=\; \tfrac{1}{N} \boldsymbol{b}^H \big(\boldsymbol{R}_b \odot \boldsymbol{A}_{\mathsf{s}} \big) \boldsymbol{b}, \tag{12}$$

$$\;=\; \tfrac{1}{N} \boldsymbol{a}^H \big(\boldsymbol{R}_a \odot \boldsymbol{B}_{\mathsf{s}} \big) \boldsymbol{a}, \tag{13}$$

where $\boldsymbol{R}_b$ and $\boldsymbol{A}_{\mathsf{s}}$ are $N_b \times N_b$ matrices defined element-wise as $[\boldsymbol{R}_b]_{m,n} := r_{\mathsf{t}}(n-m)$ and $[\boldsymbol{A}_{\mathsf{s}}]_{m,n} := \sum_{l=0}^{N_h-1} \sigma_l^2 a_{n-l} a_{m-l}^*$, and where $\boldsymbol{R}_a$ and $\boldsymbol{B}_{\mathsf{s}}$ are $N_a \times N_a$ matrices defined element-wise as $[\boldsymbol{R}_a]_{p,q} := r_{\mathsf{t}}(q-p)$ and $[\boldsymbol{B}_{\mathsf{s}}]_{p,q} := \sum_{l=0}^{N_h-1} \sigma_l^2 b_{q+l} b_{p+l}^*$.

Next we derive an expression for $\mathcal{E}_{\mathsf{ni}}$. From (5) and our definition of $\mathcal{E}_{\mathsf{ni},d}$, we have

$$\mathcal{E}_{\mathsf{ni},d} \;=\; \mathrm{E}\Big\{ \Big| w_d^{(i)} + \sum_{\ell \neq 0} \sum_{k=0}^{N-1} \breve{h}_{\mathsf{df}}^{(i,\ell)}(d-k,k) s_k^{(i-\ell)} + \sum_{k \notin \{d-D,\ldots,d+D\}} \breve{h}_{\mathsf{df}}^{(i,0)}(d-k,k) s_k^{(i)} \Big|^2 \Big\}. \quad (14)$$

Since $w_d^{(i)}, \{s_k^{(j)}\}\big|_{j \neq i}$, and $\{s_k^{(i)}\}$ are independent, and since $\{s_k^{(j)}\}$ are unit-variance i.i.d.,

$$\mathcal{E}_{\mathsf{ni},d} \;=\; \mathrm{E}\{|w_d^{(i)}|^2\} + \sum_{\ell=-L_{\mathsf{pre}}}^{L_{\mathsf{pst}}} \sum_{k=0}^{N-1} \mathrm{E}\{|\breve{h}_{\mathsf{df}}^{(i,\ell)}(d-k,k)|^2\} - \sum_{k=d-D}^{d+D} \mathrm{E}\{|\breve{h}_{\mathsf{df}}^{(i,0)}(d-k,k)|^2\} \quad (15)$$

where, from (6),

$$\mathrm{E}\{|w_d^{(i)}|^2\} \;=\; \frac{1}{N} \sum_{n,m=0}^{N_b-1} b_n b_m^* \, \mathrm{E}\{\nu_n^{(i)} \nu_m^{(i)*}\} e^{-j\frac{2\pi}{N} d(n-m)} \;=\; \frac{1}{N} \sum_{n=0}^{N_b-1} |b_n|^2 \sigma^2 \quad (16)$$

From (10), $\mathcal{E}_{\mathsf{ni}} = \sum_d \mathcal{E}_{\mathsf{ni},d}$, and the facts that $\sum_{k=0}^{N-1} \sum_{d=0}^{N-1} e^{-j\frac{2\pi}{N}(d-k)(n-m)} = N^2 \delta(\langle n-m \rangle_N)$, and $\sum_{q=-D}^{D} e^{-j\frac{2\pi}{N} q(n-m)} = \sin(\frac{\pi}{N}(2D+1)(n-m)) / \sin(\frac{\pi}{N}(n-m))$, we have

$$\begin{aligned} \mathcal{E}_{\mathsf{ni}} \;=\; & \sigma^2 \sum_{n=0}^{N_b-1} |b_n|^2 + \sum_{n=0}^{N_b-1} \sum_{m=0}^{N_b-1} b_n b_m^* r_{\mathsf{t}}(n-m) \delta(\langle n-m \rangle_N) \sum_{\ell=-L_{\mathsf{pre}}}^{L_{\mathsf{pst}}} \sum_{l=0}^{N_h-1} \sigma_l^2 a_{\ell N_s+n-l} a_{\ell N_s+m-l}^* \\ & - \sum_{n=0}^{N_b-1} \sum_{m=0}^{N_b-1} b_n b_m^* r_{\mathsf{t}}(n-m) \frac{\sin\big(\frac{\pi}{N}(2D+1)(n-m)\big)}{N \sin\big(\frac{\pi}{N}(n-m)\big)} \sum_{l=0}^{N_h-1} \sigma_l^2 a_{n-l} a_{m-l}^*. \end{aligned} \quad (17)$$

Using $\boldsymbol{b} := [b_0, \ldots, b_{N_b-1}]^t$, (17) can be put in the $N_b \times N_b$ quadratic forms (18) and (19)

$$\begin{aligned} \mathcal{E}_{\mathsf{ni}} \;&=\; \boldsymbol{b}^H \big(\sigma^2 \boldsymbol{I}_{N_b} + \boldsymbol{R}_b \odot \boldsymbol{C}_b \odot \boldsymbol{A}_{\mathsf{t}} - \boldsymbol{R}_b \odot \boldsymbol{D}_b \odot \boldsymbol{A}_{\mathsf{s}} \big) \boldsymbol{b} && (18) \\ &=\; \boldsymbol{a}^H \big(\|\boldsymbol{b}\|^2 \sigma^2 / N_s + \boldsymbol{R}_a \odot \boldsymbol{C}_a \odot \boldsymbol{B}_{\mathsf{t}} - \boldsymbol{R}_a \odot \boldsymbol{D}_a \odot \boldsymbol{B}_{\mathsf{s}} \big) \boldsymbol{a}, && (19) \end{aligned}$$

In (18), $\boldsymbol{R}_b$ and $\boldsymbol{A}_{\mathsf{s}}$ were previously defined, and $\boldsymbol{C}_b$, $\boldsymbol{D}_b$, and $\boldsymbol{A}_{\mathsf{t}}$ are $N_b \times N_b$ matrices defined element-wise as $[\boldsymbol{C}_b]_{m,n} := \delta(\langle n-m \rangle_N)$, $[\boldsymbol{D}_b]_{m,n} := \frac{1}{N} \sin(\frac{\pi}{N}(2D+1)(n-m)) / \sin(\frac{\pi}{N}(n-m))$, and $[\boldsymbol{A}_{\mathsf{t}}]_{m,n} := \sum_{\ell=-L_{\mathsf{pre}}}^{L_{\mathsf{pst}}} \sum_{l=0}^{N_h-1} \sigma_l^2 a_{\ell N_s+n-l} a_{\ell N_s+m-l}^*$. In (19), $\boldsymbol{R}_a$ and $\boldsymbol{B}_{\mathsf{s}}$ were previously defined, and $\boldsymbol{C}_a$, $\boldsymbol{D}_a$, and $\boldsymbol{B}_{\mathsf{t}}$ are $N_a \times N_a$ matrices defined element-wise as $[\boldsymbol{D}_a]_{p,q} := \frac{1}{N} \sin(\frac{\pi}{N}(2D+1)(q-p)) / \sin(\frac{\pi}{N}(q-p))$, $[\boldsymbol{B}_{\mathsf{t}}]_{p,q} := \sum_{\ell=-L_{\mathsf{pre}}}^{L_{\mathsf{pst}}} \sum_{l=0}^{N_h-1} \sigma_l^2 b_{q+l-\ell N_s} b_{p+l-\ell N_s}^*$, and $[\boldsymbol{C}_a]_{p,q} := \delta(\langle q-p \rangle_N)$. We used $\|\boldsymbol{a}\|^2 = N_s$ to write (19). Since $\mathrm{SINR} = \mathcal{E}_{\mathsf{s}} / \mathcal{E}_{\mathsf{ni}}$ is not a function of $\|\boldsymbol{b}\|$, we choose $\|\boldsymbol{b}\|^2 = N_s$ in the sequel.

To optimize $\mathrm{SINR} = \mathcal{E}_{\mathsf{s}} / \mathcal{E}_{\mathsf{ni}}$ jointly with respect to $\boldsymbol{a}$ and $\boldsymbol{b}$ under the constraints $\|\boldsymbol{a}\|^2 = \|\boldsymbol{b}\|^2 = N_s$, we alternate the pair of optimizations (20) and (21), where $\boldsymbol{v}_\star(\boldsymbol{M}, \boldsymbol{N})$ denotes the principle generalized eigenvector of the matrix pair $(\boldsymbol{M}, \boldsymbol{N})$. Recall that $\boldsymbol{A}_{\mathsf{s}}$ and $\boldsymbol{A}_{\mathsf{t}}$ are functions of $\boldsymbol{a}$ and that $\boldsymbol{B}_{\mathsf{s}}$ and $\boldsymbol{B}_{\mathsf{t}}$ are functions of $\boldsymbol{b}$. The optimization can be carried out in advance for particular fading scenarios. For example, in the case of Rayleigh fading, the pulses

depend on maximum Doppler frequency, power profile, and noise variance.

$$\begin{aligned}
\boldsymbol{b}_{\star|\boldsymbol{a}} &= \arg \max_{\boldsymbol{b}:\|\boldsymbol{b}\|^2=N_s} \frac{\boldsymbol{b}^H\big(\boldsymbol{R}_b \odot \boldsymbol{A}_{\mathsf{s}}\big)\boldsymbol{b}}{\boldsymbol{b}^H\big(\sigma^2\boldsymbol{I} + \boldsymbol{R}_b \odot \boldsymbol{C}_b \odot \boldsymbol{A}_{\mathsf{t}} - \boldsymbol{R}_b \odot \boldsymbol{D}_b \odot \boldsymbol{A}_{\mathsf{s}}\big)\boldsymbol{b}} \\
&= \boldsymbol{v}_\star\big(\boldsymbol{R}_b \odot \boldsymbol{A}_{\mathsf{s}},\ \sigma^2\boldsymbol{I} + \boldsymbol{R}_b \odot \boldsymbol{C}_b \odot \boldsymbol{A}_{\mathsf{t}} - \boldsymbol{R}_b \odot \boldsymbol{D}_b \odot \boldsymbol{A}_{\mathsf{s}}\big) \cdot \sqrt{N_s} \qquad (20) \\
\boldsymbol{a}_{\star|\boldsymbol{b}} &= \arg \max_{\boldsymbol{a}:\|\boldsymbol{a}\|^2=N_s} \frac{\boldsymbol{a}^H\big(\boldsymbol{R}_a \odot \boldsymbol{B}_{\mathsf{s}}\big)\boldsymbol{a}}{\boldsymbol{a}^H\big(\sigma^2\boldsymbol{I} + \boldsymbol{R}_a \odot \boldsymbol{C}_a \odot \boldsymbol{B}_{\mathsf{t}} - \boldsymbol{R}_a \odot \boldsymbol{D}_a \odot \boldsymbol{B}_{\mathsf{s}}\big)\boldsymbol{a}} \\
&= \boldsymbol{v}_\star\big(\boldsymbol{R}_a \odot \boldsymbol{B}_{\mathsf{s}},\ \sigma^2\boldsymbol{I} + \boldsymbol{R}_a \odot \boldsymbol{C}_a \odot \boldsymbol{B}_{\mathsf{t}} - \boldsymbol{R}_a \odot \boldsymbol{D}_a \odot \boldsymbol{B}_{\mathsf{s}}\big) \cdot \sqrt{N_s} \qquad (21)
\end{aligned}$$

3.2 Postcursor-ISI Pulse Design

The pulses described in the Sec. 3.1 were designed to suppress both pre-cursor and post-cursor ISI. With decision-feedback equalization, however, post-cursor ISI can be tolerated, allowing more freedom in pulse design.

With only a few modifications, post-cursor ISI can be incorporated into the the pulse design of Sec. 3.1. Regarding $\mathcal{E}_{\mathsf{s}}$, the definition and expressions remain the same, i.e., (12)-(13). Regarding $\mathcal{E}_{\mathsf{ni}}$, we remove the positive terms from the ℓ-summations in (14)-(15), (17), and the definitions of $\boldsymbol{A}_{\mathsf{t}}$ and $\boldsymbol{B}_{\mathsf{t}}$. Thus, the alternating optimization (20)-(21) applies after these slight redefinitions of $\boldsymbol{A}_{\mathsf{t}}$ and $\boldsymbol{B}_{\mathsf{t}}$.

4 Symbol Estimation

Here we build on the low-complexity iterative algorithms from [6, 7] which recover $\boldsymbol{s}^{(i)}$ from $\boldsymbol{x}^{(i)}$ while leveraging the quasi-banded structure of $\breve{\mathcal{H}}^{(i,0)}$. The symbols $\{s_k^{(i)}\}_{k=0}^{N-1}$ are estimated *sequentially* using a linear MMSE technique that incorporates the outcomes of previous estimates (and/or known pilots) as prior information for subsequent estimates. In doing so, we hope to avoid both the noise-enhancement of linear equalization and the error-propagation of hard decision feedback. While we avoid DFE from *within* $\boldsymbol{s}^{(i)}$, we do consider DFE cancellation of post-cursor ISI from $\{\boldsymbol{s}^{(i-\ell)}\}_{\ell=1}^{L_{\mathsf{pst}}}$. We focus on estimation rather than uncoded detection because *coded* detection performance is known to be proportional to the MSE of soft symbol estimates [15]. Coding details, however, are outside the scope of this paper.

4.1) MMSE Estimation: When the MIMO channel $\{\breve{\mathcal{H}}^{(i,\ell)}\}_{\ell=-L_{\mathsf{pre}}}^{L_{\mathsf{pst}}}$ has a cursor coefficient $\breve{\mathcal{H}}^{(i,0)}$ whose structure approximates that shown in Fig. 1, s_k will contribute primarily to the observation elements $\{\breve{x}_d\}_{d=k-D}^{k+D}$, *where all indexing in this section is taken modulo-*N. Local estimates of s_k are then generated using

$$\breve{\boldsymbol{x}}_k^{(i)} := \begin{cases} [\breve{x}_{k-D}^{(i)}, \cdots, \breve{x}_{k+D}^{(i)}]^t - \sum_{\ell=1}^{L_{\mathsf{pst}}} \breve{\mathcal{H}}^{(i,\ell)}(k-D:k+D,:)\hat{\breve{\boldsymbol{s}}}^{(i-\ell)} & \text{with DFE,} \\ [\breve{x}_{k-D}^{(i)}, \cdots, \breve{x}_{k+D}^{(i)}]^t & \text{without DFE,} \end{cases}$$

where $\{\hat{\breve{\boldsymbol{s}}}^{(i-\ell)}\}_{\ell>0}$ denotes past decisions. If we define $\boldsymbol{s}_k^{(i)} := [s_{k-2D}^{(i)}, \cdots, s_{k+2D}^{(i)}]^t$, $\boldsymbol{w}_k^{(i)} := [w_{k-D}^{(i)}, \cdots, w_{k+D}^{(i)}]^t$, and $\breve{\mathcal{H}}_k^{(i)} := \breve{\mathcal{H}}^{(i,0)}(k-D:k+D, k-2D:k+2D)$, then we can write

$$\breve{\boldsymbol{x}}_k^{(i)} = \breve{\mathcal{H}}_k^{(i)}\boldsymbol{s}_k^{(i)} + \boldsymbol{\varepsilon}_k^{(i)}, \qquad (22)$$

where $\boldsymbol{\varepsilon}_k^{(i)}$ denotes noise plus residual ICI and ISI (consisting only of precursor and error-propagation components in the DF case). Note that, as a consequence of modulo-N indexing,

the elements of $\breve{\mathcal{H}}^{(i,0)}$ from the top-right and bottom-left shaded triangles in Fig. 1 are included in $\breve{\mathcal{H}}_k^{(i)}$. In the sequel, we omit the superscript indices.

The MMSE linear estimate of s_k given $\breve{\boldsymbol{x}}_k$ is

$$\hat{s}_k \;=\; \mathrm{E}\{s_k\} + \mathrm{Cov}(s_k, \breve{\boldsymbol{x}}_k)\,\mathrm{Cov}(\breve{\boldsymbol{x}}_k, \breve{\boldsymbol{x}}_k)^{-1}\big(\breve{\boldsymbol{x}}_k - \mathrm{E}\{\breve{\boldsymbol{x}}_k\}\big). \tag{23}$$

Our assumptions imply $\mathrm{E}\{\boldsymbol{\varepsilon}_k\} = \mathbf{0}$ and $\mathrm{E}\{\boldsymbol{s}_k\boldsymbol{\varepsilon}_k^H\} = \mathbf{0}$. If we define $\boldsymbol{\Sigma}_k := \mathrm{E}\{\boldsymbol{\varepsilon}_k\boldsymbol{\varepsilon}_k^H\}$, $\breve{\boldsymbol{h}}_k := [\breve{h}_{k-D,k}^{(i,0)}, \cdots, \breve{h}_{k+D,k}^{(i,0)}]^t$, $\bar{s}_k := \mathrm{E}\{s_k\}$, $v_k := \mathrm{Cov}(s_k, s_k)$, $\bar{\boldsymbol{s}}_k := [\bar{s}_{k-2D}, \ldots, \bar{s}_{k+2D}]^t$, and $\boldsymbol{v}_k := [v_{k-2D}, \ldots, v_{k+2D}]^t$, then it is straightforward to show that $\mathrm{E}\{\breve{\boldsymbol{x}}_k\} = \breve{\mathcal{H}}_k\bar{\boldsymbol{s}}_k$, $\mathrm{Cov}(s_k, \breve{\boldsymbol{x}}_k) = v_k\breve{\boldsymbol{h}}_k^H$, and $\mathrm{Cov}(\breve{\boldsymbol{x}}_k, \breve{\boldsymbol{x}}_k) = \boldsymbol{\Sigma}_k + \breve{\mathcal{H}}_k\,\mathcal{D}(\boldsymbol{v}_k)\breve{\mathcal{H}}_k^H$, giving the MMSE estimate

$$\hat{s}_k \;=\; \bar{s}_k + \boldsymbol{f}_k^H(\breve{\boldsymbol{x}}_k - \breve{\mathcal{H}}_k\bar{\boldsymbol{s}}_k). \tag{24}$$

$$\boldsymbol{f}_k \;=\; \big(\boldsymbol{\Sigma}_k + \breve{\mathcal{H}}_k\,\mathcal{D}(\boldsymbol{v}_k)\breve{\mathcal{H}}_k^H\big)^{-1}\breve{\boldsymbol{h}}_k v_k. \tag{25}$$

We choose to use only *extrinsic* information, i.e., only the priors from $\{s_d\}_{d\neq k}$ when estimating s_k. This can be accomplished using (24)-(25) with $\bar{s}_k = 0$ and $v_k = 1$.

Numerical studies have shown that, when the pulse shapes are designed as in Sec. 3, Σ_k is dominated by its noise component. It can be shown that the noise component of Σ_k is a Toeplitz matrix invariant to k.

4.2) Update of the Priors: The symbol estimate $\hat{s}_k$ can be used to update $\bar{s}_k$ and v_k. For simplicity, we consider only i.i.d. BPSK symbols $s_k \in \mathcal{B} := \{-1, +1\}$; QAM extensions are straightforward. We assume a conditionally Gaussian model for the estimates, i.e., $p(\hat{s}_k|s_k = b) \approx \phi\big((\hat{s}_k - \mu_k(b))/\sigma_k(b)\big)/\sigma_k(b)$, where $\phi(w) := e^{-w^2}/\sqrt{\pi}$ is the proper complex Gaussian density. Defining $\mu_k(b) := \mathrm{E}\{\hat{s}_k|s_k = b\}$ and $\sigma_k^2(b) := \mathrm{Cov}(\hat{s}_k, \hat{s}_k|s_k = b)$, it can be shown that $\mu_k(b) = \boldsymbol{f}_k^H\breve{\boldsymbol{h}}_k \cdot b$ and $\sigma_k^2(b) = \boldsymbol{f}_k^H\breve{\boldsymbol{h}}_k(1 - \breve{\boldsymbol{h}}_k^H\boldsymbol{f}_k)$. If we define the prior and posterior log-likelihood ratios (LLR) as $L(s_k) := \ln\frac{P(s_k=+1)}{P(s_k=-1)}$ and $L(s_k|\hat{s}_k) := \ln\frac{P(s_k=+1|\hat{s}_k)}{P(s_k=-1|\hat{s}_k)}$, respectively, their difference can be expressed as

$$\Delta L(\hat{s}_k) \;:=\; L(s_k|\hat{s}_k) - L(s_k) \;=\; 4\,\mathrm{Re}(\hat{s}_k)/(1 - \breve{\boldsymbol{h}}_k^H\boldsymbol{f}_k). \tag{26}$$

The posterior LLR leads to an update of the priors:

$$L_{\mathsf{new}}(s_k) \;=\; L(s_k) + \Delta L(\hat{s}_k) \tag{27}$$

$$\bar{s}_{k,\mathsf{new}} \;=\; \textstyle\sum_{b\in\mathcal{B}} b\cdot P(s_k = s|\hat{s}_k) \;=\; \tanh(L_{\mathsf{new}}(s_k)/2) \tag{28}$$

$$v_{k,\mathsf{new}} \;=\; \textstyle\sum_{b\in\mathcal{B}}(b - \mathrm{E}\{s_k|\hat{s}_k\})^2\cdot P(s_k = b|\hat{s}_k) \;=\; 1 - \bar{s}_{k,\mathsf{new}}^2 \tag{29}$$

which, in turn, can be used to estimate $\{s_d\}_{d\neq k}$ via (24)-(25).

4.3) Iteration: We initially set $\bar{s}_k = 0$ and $v_k = 1$ (though pilots could be handled by setting $\bar{s}_k = s_k$ and $v_k = 0$). For *sequential iterative estimation* (SIE), we calculate $\hat{s}_0$ via (24)-(25) and then immediately update the priors $\bar{s}_0$ and v_0 via (26)-(27). Next, we calculate $\hat{s}_1$ and then immediately update $\bar{s}_1$ and v_1. This continues until $\hat{s}_{N-1}$, $\bar{s}_{N-1,\mathsf{new}}$, and $v_{N-1,\mathsf{new}}$ have been computed, then repeats again, starting with $\hat{s}_0$. The algorithm terminates after a specified number of iterations or when the LLRs surpass a threshold.

A simplification called *sequential decision feedback* (SDF) operates identically to SIE except that $\bar{s}_{k,\mathsf{new}} = \mathrm{sgn}(\hat{s}_k)$ and $v_{k,\mathsf{new}} = 0$. Computation of LLRs is not necessary and the algorithm terminates after a specified number of iterations or when $\{\bar{s}_k\}$ converge.

4.4) Comments: The computational complexity of SIE and SDF, dominated by the $(2D{+}1)\times(2D{+}1)$ matrix inversion in (25), is $\mathcal{O}(D^2N)$ multiplications per iteration.

SIE is related to the estimation stage of the "turbo equalization" scheme [16]. Unlike SIE, however, [16] assumes a LTI channel in white noise and inserts a decoding iteration after each equalization iteration. SDF is reminiscent of the "successive detection" scheme used in [17], though SDF does not employ an $\mathcal{O}(N^2)$ symbol ordering procedure. Also, SDF employs multiple iterations so that hard decisions can converge.

5 Simulations

To evaluate the iterative equalization algorithms, we compare $\frac{1}{N}\sum_{k=0}^{N-1}\mathrm{E}\{|s_k^{(i)}-\hat{s}_k^{(i)}|^2\}$, their average MSE, to that of the matched filter bound (MFB), i.e., the MMSE estimation of $s_k^{(i)}$ assuming all interference $\{s_d^{(j)}\}_{(j,d)\neq(i,k)}$ is known perfectly. We also consider an *approximate* MFB (AMFB) which assumes that, when estimating $s_k^{(i)}$, only neighboring co-cursor interference $\{s_d^{(i)}\}_{d=k-2D}^{k+2D}$ is known; ISI and non-neighboring ICI are unknown. This AMFB lower bounds the MSE of the iterative algorithms, and the AMFB/MFB difference measures the pulse design's success in suppressing out-of-target interference.

The MFB itself is a function of the pulse design. We compare the MFB for our PS-FDM to the following SVD-based scheme, which requires transmitter channel *realization* knowledge (as opposed to *statistical* knowledge). Denote by $\mathcal{H}_{\mathsf{tl}}^{(i)}$ the $N_b \times N_a$ convolution matrix constructed from $\{h_{\mathsf{tl}}(n,:)\}_{n=iN_s}^{iN_s+N_b}$ where the coefficients in $\mathcal{H}_{\mathsf{tl}}^{(i)}$ are exactly those used to construct $\{\breve{\mathcal{H}}^{(i,\ell)}\}_{\ell=-L_{\mathsf{pre}}}^{L_{\mathsf{pst}}}$. Then define the modulation waveforms for $\{s_k^{(i)}\}_{k=0}^{N-1}$ as the first N right singular vectors of $\mathcal{H}_{\mathsf{tl}}^{(i)}$ (scaled by $\sqrt{N_s/N}$ for fair comparison) and the corresponding matched filters for estimation of $\{s_k^{(i)}\}_{k=0}^{N-1}$ by the first N left singular vectors of $\mathcal{H}_{\mathsf{tl}}^{(i)}$. Though our choices of N_a and N_b promote ISI, we assume this ISI is known in our evaluation of the "SVD-MFB."

Experiments employ i.i.d. BPSK, SNR^{-1}-variance circular AWGN noise, a WSSUS Rayleigh-fading channel with $\sigma_l^2 = N_h^{-1}$ (for $0 \le l < N_h$), and the design choices $N_a = 1.5N_s$, $N_b = N_a + N_h/2$, and $D = \lceil f_{\mathsf{d}} N \rceil + 1$. Unless otherwise noted, assume $N = 64$, $N_h = 16$, $N_s = N$ (i.e., no guard interval), and $f_{\mathsf{d}} = 0.03$. Channel knowledge is assumed and so no pilots were employed. SIE and SDF were allowed 4 iterations, and performance was averaged over 5000 multicarrier symbols. Recall that f_{d} has been normalized to the *channel-use* interval as opposed to the multicarrier-symbol interval.

Figure 1(a) plots typical pulse shapes for the ISI-free target (i.e., no DFE) while Fig. 1(b) plots them for the post-cursor ISI target (i.e., for DFE). Note that the pulses may include negative values and may be asymmetric in the DFE case, and that our choices for N_a and N_b appear to be "large enough."

Figure 3 shows MSE vs. SNR for PS-FDM without DFE at various Dopplers; SIE and SDF are compared to the PS-AMFB, PS-MFB, and SVD-MFB. At all f_{d}, we see AMFB=MFB, meaning that out-of-target ICI/ISI is negligible. SIE reaches the MFB in all but the $f_{\mathsf{d}} = 0.1$/SNR$\le$5dB case, whereas SDF reaches the MFB only at $f_{\mathsf{d}} = 0.01$; this is remarkable considering that SIE is $\mathcal{O}(N)$. The SNR gap between PS-MFB and SVD-MFB is about 3dB at $f_{\mathsf{d}} = 0.01$ but shrinks to about 1dB at $f_{\mathsf{d}} = 0.1$; recall that, as f_{d} increases, D also increases and so provides more diversity at the cost of higher implementation complexity. Results for the same setup but *with* DFE (not shown here) are nearly identical since this relatively small delay spread does not generate much ISI.

Figure 4 shows MSE vs. SNR for various choices of multicarrier-symbol interval N_s (recalling that each multicarrier symbol contains $N = 64$ BPSK symbols). Here AMFB=MFB in all but the high-SNR region of the "overloaded" case $N_s = 0.75N$. SIE performs near to the MFB in all but the low-SNR case and the high-SNR overloaded case, whereas SDF lags behind

1-2dB. Note that the gap between SVD-MFB and PS-MFB closes in the overloaded case; the orthogonality of the SVD basis is suboptimal as far as the MFB concerns. We conclude that PS-FDM is robust to a lack of guard interval (i.e., $N_s \leq N$). The DFE results (not shown here) are nearly identical.

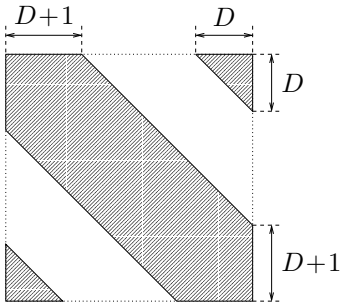

Figure 1: Desired structure of MIMO cursor coefficient $\breve{\mathcal{H}}^{(i,0)}$. Typically, $D = \lceil f_{\mathsf{d}} N \rceil + 1$.

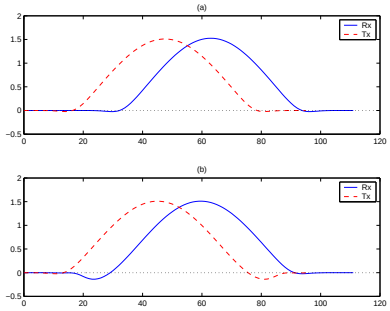

Figure 2: Pulses for (a) non-DFE (b) DFE target, with $N_h = 32$ and SNR=20 dB.

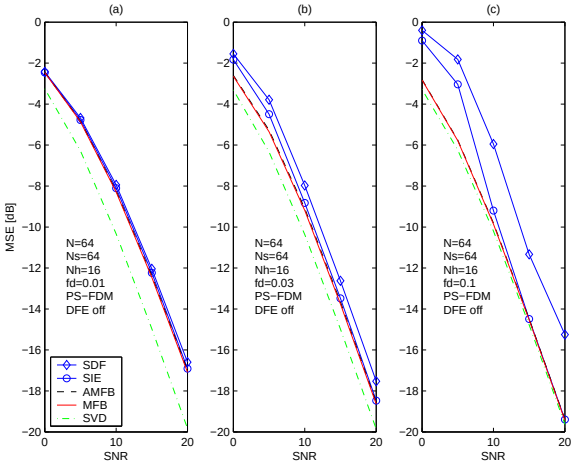

Figure 3: MSE versus SNR for Doppler (a) $f_{\mathsf{d}} = 0.01$, (b) $f_{\mathsf{d}} = 0.03$, and (c) $f_{\mathsf{d}} = 0.1$.

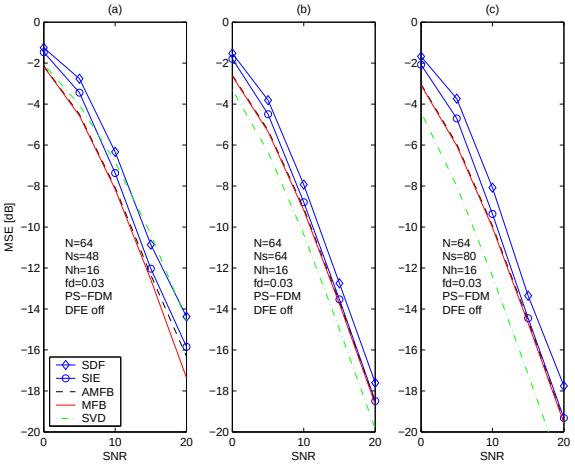

Figure 4: MSE versus SNR for guard interval (a) $N_g = -16$, (b) $N_g = 0$, and (c) $N_g = 16$.

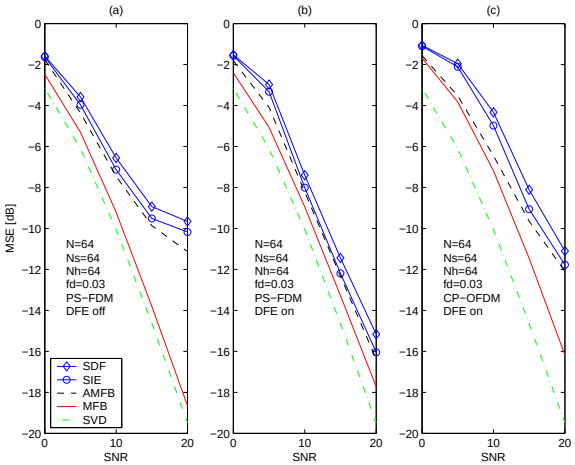

Figure 5: MSE versus SNR for $N_h = 64$ and (a) PS-FDM without DFE, (b) PS-FDM with DFE, and (c) CP-OFDM with DFE.

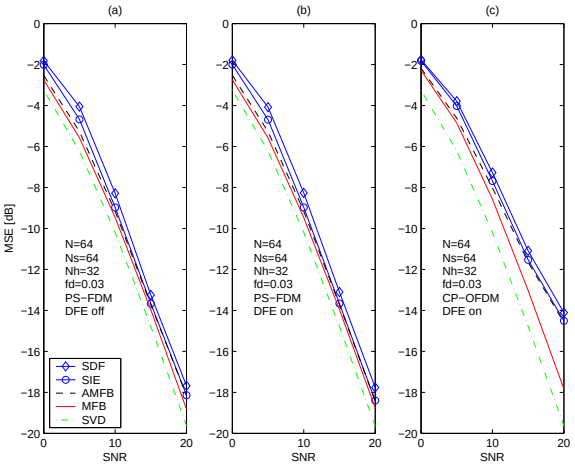

Figure 6: MSE versus SNR for $N_h = 32$ and (a) PS-FDM without DFE, (b) PS-FDM with DFE, and (c) CP-OFDM with DFE.

Figure 5 compares various schemes under large delay spread $N_h = N_s = N = 64$. For PS-FDM without DFE, there is a large gap between the MFB and AMFB: out-of-target ISI/ICI is not well suppressed. Adding DFE to PS-FDM, the MFB/AMFB gap closes to <2dB and SIE nearly reaches the AMFB. For CP-OFDM with DFE, we see relatively large MFB/AMFB

and PS-MFB/SVD-MFB gaps. Repeating the experiment with $N_h = 32$ (see Fig. 6), we find that PS-FDM gives excellent—and nearly identical—performance with or without DFE, while CP-OFDM with DFE still displays a large AMFB/MFB gap. We conclude that PS-FDM is quite robust to delay spread, though the DFE option should be exercised when $N_h \geq N_s$.

6 Conclusions

We presented a new approach to PS-FDM in the presence of doubly-dispersive fading. Pulse sequences were constructed to shape ICI/ISI into a pattern that enables low-complexity diversity-leveraging equalization, and a suitable equalization algorithm was described. Simulations demonstrated the efficacy of the proposed technique.

References

[1] S. B. Weinstein and P. M. Ebert, "Data transmission by frequency division multiplexing using the discrete Fourier transform," *IEEE Trans. Commun.*, vol. 19, pp. 628–634, Oct. 1971.

[2] A. Stamoulis, S. N. Diggavi, and N. Al-Dhahir, "Intercarrier interference in MIMO OFDM," *IEEE Trans. Signal Processing*, vol. 50, pp. 2451–2464, Oct. 2002.

[3] X. Cai and G. B. Giannakis, "Bounding performance and suppressing inter-carrier interference in wireless mobile OFDM," *IEEE Trans. Commun.*, vol. 51, pp. 2047–2056, Dec. 2003.

[4] W. Burchill and C. Leung, "Matched filter bound for OFDM on Rayleigh fading channels," *Electronics Letters*, vol. 31, pp. 1716–1717, Sep. 1995.

[5] A. M. Sayeed and B. Aazhang, "Joint multipath-doppler diversity in mobile wireless communications," *IEEE Trans. Commun.*, vol. 47, pp. 123–132, Jan. 1999.

[6] P. Schniter, "A low-complexity receiver for OFDM in doubly-selective channels," in *Proc. IEEE Global Telecommunications Conf.*, 2003. (to appear).

[7] P. Schniter, "Low-complexity equalization of OFDM in doubly-selective channels," *IEEE Trans. Signal Processing*, vol. 52, pp. 1002–1011, Apr. 2004.

[8] B. Le Floch, M. Alard, and C. Berrou, "Coded orthogonal frequency division multiplex," *Proc. IEEE*, vol. 83, pp. 982–996, June 1995.

[9] R. Haas and J.-C. Belfiore, "A time-frequency well-localized pulse for multiple carrier transmission," *Wireless Personal Commun.*, vol. 5, pp. 1–18, 1997.

[10] K. Matheus and K.-D. Kammeyer, "Optimal design of a multicarrier systems with soft impulse shaping including equalization in time or frequency direction," in *IEEE Globecom*, vol. 1, pp. 310–314, 1997.

[11] W. Kozek and A. F. Molisch, "Nonorthogonal pulseshapes for multicarrier communications in doubly dispersive channels," *IEEE J. Select. Areas In Commun.*, vol. 16, pp. 1579–1589, Oct. 1998.

[12] H. Bölcskei, "Orthogonal frequency division multiplexing based on offset QAM," in *Advances in Gabor Theory* (H. G. Feichtinger and T. Strohmer, eds.), pp. 321–352, Birkhäuser, 2002.

[13] Y. Sun, "Bandwidth-efficient wireless OFDM," *IEEE J. Select. Areas In Commun.*, vol. 19, pp. 2267–2278, Nov. 2001.

[14] J. G. Proakis, *Digital Communications*. New York: McGraw-Hill, 4th ed., 2001.

[15] H. Sari, G. Karam, and I. Jeanclaude, "Transmission techniques for digital terrestrial TV broadcasting," *IEEE Commun. Mag.*, pp. 100–109, Feb. 1995.

[16] M. Tüchler, A. Singer, and R. Koetter, "Minimum mean square error equalization using *a priori* information," *IEEE Trans. Signal Processing*, vol. 50, pp. 673–683, Mar. 2002.

[17] Y.-S. Choi, P. J. Voltz, and F. A. Cassara, "On channel estimation and detection for multicarrier signals in fast and selective Rayleigh fading channels," *IEEE Trans. Commun.*, vol. 49, pp. 1375–1387, Aug. 2001.